PCCP

ROYAL SOCIETY OF CHEMISTRY

PAPER

View Article Online
View Journal | View Issue

Cite this: *Phys. Chem. Chem. Phys.*, 2025, **27**, 6465

Effect of architectural asymmetry of hyperbranched block copolymers on their phase boundaries†

Jiahao Shi, [a] Qingshu Dong, *[a] Tao Yang [b] and Weihua Li *[a]

Asymmetric architecture of AB-type block copolymers can induce additional spontaneous curvature to the A/B interface, accordingly deflecting the phase boundaries. However, it is often difficult to determine or compare the asymmetric effects of different asymmetric architectures. In this work, we proposed to use the equivalent arm number n_{equ}, which was originally defined as $n_{equ} = n/iĐ$ for AB_n with unequal B-arms and iĐ being the intramolecular polydispersity of these B-arms, to quantify the asymmetric effect of various linear-hyperbranched copolymers. For each linear-hyperbranched copolymer, n_{equ} is estimated by matching its phase boundaries on the side with expanded spherical phase region with those of AB_n with unequal B-arms but tunable iĐ. Our results suggest that the addition of B-blocks at the further location from the A–B joint point has less influence on n_{equ}, *i.e.* the asymmetric effect, because these B-blocks can access more space. For the linear-dendrimer copolymers, n_{equ} changes from 2 to about 3.8 when the overall generation number of the copolymer increases from 2 to 5. In other words, the asymmetric effect of these linear-dendrimer copolymers is intermediate between those of AB_2 and AB_4 miktoarm star copolymers. In brief, n_{equ} can effectively describe the asymmetric effect on the interfacial curvature of complex asymmetric architectures.

Received 22nd December 2024,
Accepted 3rd March 2025

DOI: 10.1039/d4cp04814h

rsc.li/pccp

1 Introduction

Block copolymers can self-assemble into innumerable ordered structures when varying their composition and architectures,[1–9] and thus have attracted abiding interest[10–16] in many fields including functional nanomaterials and nanotechnology.[17–20] AB diblock copolymers as the simplest block copolymer can form sphere, cylinder, network and lamellar structures as their composition changes from asymmetric to symmetric.[21–30] If there are no other different properties between A and B blocks in the AB diblock, the phase diagram with respect to the composition (or the volume fraction of A-block, f) is symmetric.[31] On both sides of the symmetric phase diagram, the spherical phase region is rather narrow and is mainly occupied by the body-centered cubic (BCC) phase. To expand the spherical region, an additional asymmetry factor needs to be introduced, such as the conformational asymmetry[32–38] or architectural asymmetry.[39–49] One of the common asymmetric architectures is AB_n miktoarm star copolymers composed of a single A block connected with n B blocks.[47,48,50–52] The multiple B blocks are more difficult to be stretched than the single A block, creating a tendency for the A/B interface to curve toward the A block. In other words, a curvature effect is caused by the branching architecture in addition to that arising from the compositional asymmetry. As a result, the phase diagram becomes asymmetric and is deflected to large volume fraction f of the A-block, of which the phase region of the A-sphere is expanded while that of the B-sphere is compressed. More importantly, the complex Frank–Kasper σ or A15 phase is stabilized with the expansion of the spherical region.[42,47,53–55]

Conformational asymmetry is related to the different intrinsic properties of flexibility, which can also be encoded into the asymmetry of the phase diagram. Almdal *et al.* proposed the ratio of Kuhn length b_A/b_B to describe the conformational asymmetry of the linear AB diblock by comparing the radius of gyration (R_g) of the linear A-block and B-block.[32] The asymmetry parameter of the AB diblock was updated as $\rho_A b_A^2/\rho_B b_B^2$, where ρ_κ (κ = A or B) is the density of the κ-monomer.[33,56] Soon after, Milner combined conformational asymmetry and architectural asymmetry into an asymmetry parameter, $\varepsilon \equiv (n_B/n_A)(\rho_A b_A^2/\rho_B b_B^2)^{0.5}$, in an AB-type miktoarm star copolymer composed of n_A A-arms and n_B B-arms.[50] This unified definition implies that the ratio of arm numbers and that of Kuhn lengths should have a similar effect

[a] *State Key Laboratory of Molecular Engineering of Polymers, Key Laboratory of Computational Physical Sciences, Research Center of AI for Polymer Science, Department of Macromolecular Science, Fudan University, Shanghai 200433, China. E-mail: qsdong@fudan.edu.cn, weihuali@fudan.edu.cn*

[b] *School of Physics, Ningxia University, Yinchuan 750021, China*

† Electronic supplementary information (ESI) available. See DOI: https://doi.org/10.1039/d4cp04814h

on the phase behavior, which has been confirmed in subsequent experimental[57–60] and theoretical studies.[37,43,48]

Besides the miktoarm star architectures, there are many other asymmetric architectures, and for some of them it is difficult to judge their degree of asymmetry (*e.g.* their deflection degree to the phase diagram). Some effort has been devoted to quantifying the asymmetry degrees of various complex AB-type block copolymers.[44,51,61–63] For example, Fredrickson *et al.*[44] attempted to calculate the asymmetry parameter of comblike/bottlebrush block copolymers by approximately computing the radius of gyration of the A and B blocks. Their asymmetry parameter can describe the deflection degree to the phase diagram for the comblike copolymers well, but not for the bottlebrush copolymers. In our previous work,[51] we proposed the number of equivalent (or effective) arms (n_{equ}) as an asymmetry parameter with reference to AB_n miktoarm star copolymers of equal arms, and used it to quantify the deflection degree of the phase diagrams of AB_n of unequal arms. We found that n_{equ} can be simply expressed as $n_{equ} = n/iĐ$, where iĐ represents the intramolecular polydispersity of the multiple arms. Our self-consistent field theory (SCFT) results demonstrate that various AB_n of unequal arms with different n but with equal n_{equ} exhibit very similar asymmetric phase diagrams, verifying that n_{equ} is an efficient asymmetry parameter for measuring the effect of asymmetric architectures on the deflection of the phase diagrams. In line with Milner's description,[50] we can combine conformational asymmetry with architectural asymmetry, then modify the equation for determining the equivalent ε (ε_{equ}) of linear-hyperbranched copolymers: $\varepsilon_{equ} = n_{equ}(\rho_A b_A^2/\rho_B b_B^2)^{0.5}$. For the linear-hyperbranched copolymers studied in this paper, we set $\rho_A = \rho_B$ and $b_A = b_B$, thus $n_{equ} = \varepsilon_{equ}$. The $n_{equ}(\varepsilon_{equ})$ is mainly reflected in the change of spontaneous curvature for the AB-type copolymer, and the most prominent manifestation is its influence on the sphere/cylinder phase boundary. Therefore, in this work, we attempt to extend the concept of n_{equ} to other asymmetric block copolymers to quantify their architectural asymmetry.

Hyperbranched copolymers including dendrimer-like have been extensively studied due to their unique architectures.[42,46,64–78] Grason *et al.*[42,46] proposed that the block copolymer composed of linear A-block and hyperbranched B-blocks exhibits a significantly amplified effect of spontaneous curvature toward the A-domain. As a result, the phase boundaries of these linear-hyperbranched copolymers are notably deflected to large volume fraction of the A-block (f), and the Frank–Kasper spherical A15 phase was predicted to be stable in the expanded region of the A-sphere.[42,47] Although the architectures are notably asymmetric, it is still difficult to determine how large their asymmetry degrees are, for example by comparing them with those of AB_n miktoarm star architectures. In this work, we will determine the equivalent arm number n_{equ} by comparing the phase boundaries of various hyperbranched copolymers to those of different AB_n with equal or unequal arms using SCFT. We first move the two B-arms of the equal-arm-AB_4 or unequal-arm-AB_4 architecture along the other two B-arms to obtain a series of linear-hyperbranched block copolymers (Fig. 1), thus determining their n_{equ}. With the arm length ratios of 1 : 1 : 2 : 2,

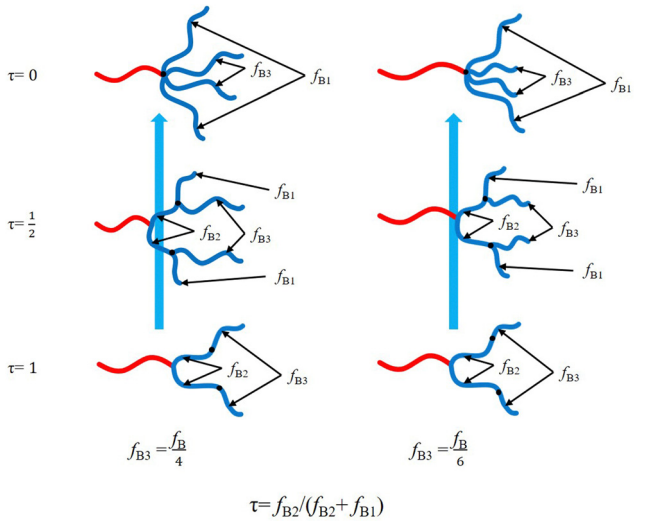

Fig. 1 Schematics of the linear-hyperbranched architectures generated from AB_n with equal or unequal B arms.

the ideal linear-dendrimer architecture can be generated from AB_4 when the two short B-arms are moved to the middle points of the other two B-arms, respectively. Then we propose a simple expression for n_{equ} with respect to the tethering position, which can reasonably measure the asymmetry degrees of these different linear-hyperbranched copolymers.

2 Theory and method

We consider an incompressible melt of volume V consisting of n_C chains of hyperbranched copolymers or AB_n. To give prominence to the architectural effect on the self-assembly behavior, we simply assume that all segments have the same Kuhn length b and density ρ_0. Each copolymer is composed of N segments in total, of which the A-block contains fN segments. Within the framework of SCFT for the Gaussian chain, the free energy functional per chain at temperature T is given by[79,80]

$$\frac{F}{n_C k_B T} = -\ln Q + \frac{1}{V}\int d\mathbf{r}\{\chi N\phi_A(\mathbf{r})\phi_B(\mathbf{r}) - w_A(\mathbf{r})\phi_A(\mathbf{r}) - w_B(\mathbf{r})\phi_B(\mathbf{r}) - \xi(\mathbf{r})[1-\phi_A(\mathbf{r})-\phi_B(\mathbf{r})]\} \quad (1)$$

where k_B is the Boltzmann constant. $\phi_\kappa(\mathbf{r})$ and $w_\kappa(\mathbf{r})$ (κ = A, B) are the volume-fraction function and the conjugate potential field of the κ-component, respectively. $\xi(\mathbf{r})$ is a Lagrange multiplier used to enforce the incompressibility condition, $\phi_A(\mathbf{r}) + \phi_B(\mathbf{r}) = 1$. The quantity Q is the partition function of one single chain interacting with the mean fields of $w_\kappa(\mathbf{r})$ (κ = A, B), which is determined by

$$Q = \frac{1}{V}\int d\mathbf{r} q(\mathbf{r}, s) q^\dagger(\mathbf{r}, s) \quad (2)$$

where $q(\mathbf{r}, s)$ and $q^\dagger(\mathbf{r}, s)$ are two conjugate propagator functions satisfying the modified diffusion equations

$$\frac{\partial q(\mathbf{r}, s)}{\partial s} = \nabla^2 q(\mathbf{r}, s) - w(\mathbf{r}, s) q(\mathbf{r}, s) \quad (3)$$

$$-\frac{\partial q^{\dagger}(\mathbf{r},s)}{\partial s} = \nabla^2 q^{\dagger}(\mathbf{r},s) - w(\mathbf{r},s)q^{\dagger}(\mathbf{r},s) \quad (4)$$

where $w(\mathbf{r}, s) = w_{\kappa}(\mathbf{r})$ when s belongs to the κ-block (κ = A, B). The values of $q(\mathbf{r}, s)$ or $q^{\dagger}(\mathbf{r}, s)$ at the free ends are set to 1 as the initial conditions. The spatial length is rescaled by the radius of gyration (R_g) of an unperturbed linear homopolymer chain with N segments, $R_g = N^{1/2}b/\sqrt{6}$. We considered that A and B segments have the same segment density ($\rho_A = \rho_B$) and length ($b_A = b_B$). The total number of segments in the A block and B blocks is given by $f_A N$ ($f_A = f$) and $f_B N$, respectively. Minimization of the free energy functional with respect to the volume-fraction functions and the mean fields leads to the following SCFT equations

$$w_A(\mathbf{r}) = \chi N \phi_B(\mathbf{r}) + \xi(\mathbf{r}) \quad (5)$$

$$w_B(\mathbf{r}) = \chi N \phi_A(\mathbf{r}) + \xi(\mathbf{r}) \quad (6)$$

$$\phi_A(\mathbf{r}) = \frac{1}{Q}\int_{s\in A} \mathrm{d}s q(\mathbf{r},s)q^{\dagger}(\mathbf{r},s) \quad (7)$$

$$\phi_B(\mathbf{r}) = \frac{1}{Q}\int_{s\in B} \mathrm{d}s q(\mathbf{r},s)q^{\dagger}(\mathbf{r},s) \quad (8)$$

$$1 = \phi_A(\mathbf{r}) + \phi_B(\mathbf{r}) \quad (9)$$

We use the pseudospectral method[81–83] to solve the modified diffusion equations, and implement the Anderson mixing iteration scheme[84] to accelerate the converging process toward the equilibrium solution. We consider eight ordered phases, including face-centered cubic (FCC) spherical phase, body-centered cubic (BCC) spherical phase, Frank–Kasper σ/A15 spherical phase, hexagonal cylinder phase (C_6), *Fddd* network phase (O^{70}), double-gyroid network phase (G) and lamellar phase (L) (Fig. 2). It is necessary to mention that we do not consider the hexagonally close-packed (HCP) spherical phase because it is nearly degenerate with the FCC phase. The sizes of the unit cell (l_x, l_y and l_z) are optimized by the variable cell algorithm.[85–87] The chain contour is divided into pieces with $\Delta s \leq 0.005$. The grid spacings Δx, Δy and Δz are chosen to be smaller than $0.15R_g$ by using a lattice of $64 \times 64 \times 64$ for the three-dimensional phases except for a lattice of $256 \times 256 \times 128$ for the σ phase and a lattice of $32 \times 64 \times 128$ for the O^{70} phase. In addition, the pseudospectral method is accelerated using the crystallographic FFT to replace the normal FFT.[88]

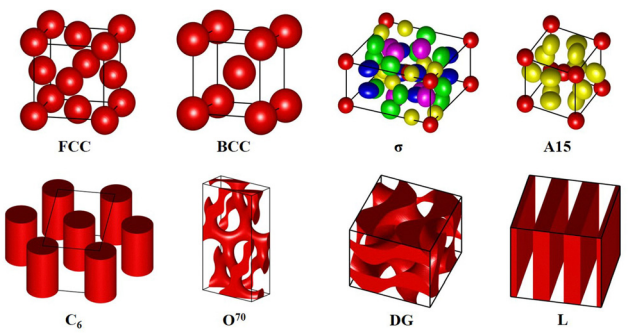

Fig. 2 Isosurface plots of the candidate ordered phases considered in the current study, including FCC, BCC, σ, A15, hexagonally arranged cylinders (C_6), *Fddd* network (O^{70}), double-gyroid (G) and lamellae (L). Larger and clearer figures and specific parameters are provided in the ESI.†

3 Results and discussion

We first consider a linear-hyperbranched architecture composed of a linear A-block connected with two generations of hyperbranched B-blocks. As shown in Fig. 1, this copolymer can be seen as an AB_2 copolymer tethered by an additional B-block on each branching B-block. The tethering B-block with volume fraction of f_{B3} divides the branching B-block of AB_2 into two sub-blocks denoted as B1 (with free end) and B2 (connected with A block) blocks with volume fractions f_{B1} and f_{B2}, respectively. We introduce a variable $\tau = f_{B2}/(f_{B2} + f_{B1})$ to characterize the tethering position of the B3-block. Accordingly, the linear-hyperbranched copolymer is reduced to AB_2 with two equal B-arms at $\tau = 1$ and AB_4 with equal or unequal B-arms at $\tau = 0$, respectively. The simple analysis implies that the asymmetry degree of this complex architecture should lie between those of AB_2 and AB_4 copolymers.

Besides the tethering position, another characteristic parameter is the ratio of B3-block. In this work, we consider two specific cases: $f_{B3} = f_B/4$ and $f_{B3} = f_B/6$. In the first case of $f_{B3} = f_B/4$, the linear-hyperbranched architecture is reduced to AB_4 of equal arms. In the other case of $f_{B3} = f_B/6$, the architecture of the B-blocks becomes dendrimer-like at $\tau = 1/2$.

To demonstrate the change of the architecture on the asymmetry, we vary τ (*i.e.* the tethering position of B3-block) to gradually change the linear-hyperbranched architecture and construct the phase diagrams with respect to f and χN. Fig. 3 presents the phase diagrams of the linear-hyperbranched copolymer with $f_{B3} = f_B/4$ for $\tau = 0$, $\tau = 1/3$, $\tau = 2/3$ and $\tau = 1$, respectively. At $\tau = 0$, the copolymer is AB_4 of equal arms, and thus its phase diagram is rather largely deflected to large f. Accordingly, the overall phase region of the A-sphere is expanded to range from $f \approx 0.172$ to $f \approx 0.344$ with a width of about $\Delta f \approx 0.172$ at $\chi N = 40$, consisting of a wide window of Frank–Kasper σ-phase as well as a considerable window of A15-phase. As the two B3-blocks (two of B-arms) move away from the junction point to the tethering positions of $\tau = 1/3$, the asymmetry of the phase diagram is noticeably reduced, accompanied by a narrowing of the A-spherical phase region. In particular, the width of the A15-phase window is decreased from $\Delta f \approx 0.041$ at $\tau = 0$ to $\Delta f \approx 0.018$ at $\tau = 1/3$. When the B3-blocks move to $\tau = 2/3$, the asymmetry or deflection of the phase diagram is further decreased, leading to the absence of the A15-phase region. Finally, the architecture changes to AB_2 at $\tau = 1$, whose phase diagram is considerably less asymmetric than that of AB_4 at $\tau = 0$. The width of the A-spherical phase region at $\chi N = 40$ is narrowed to be $\Delta f \approx 0.127$.

Qualitatively, the decrease in the asymmetry of the phase diagram with increasing τ can be explained by the change in the overall extension distance[8] of the B-blocks from the A/B

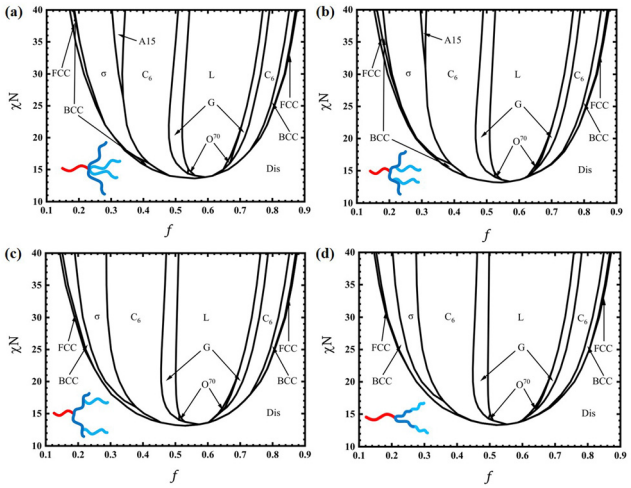

Fig. 3 Phase diagrams for copolymers with (a) τ = 0, (b) τ = 1/3, (c) τ = 2/3, and (d) τ = 1. In all cases, $f_{B3} = f_B/4$.

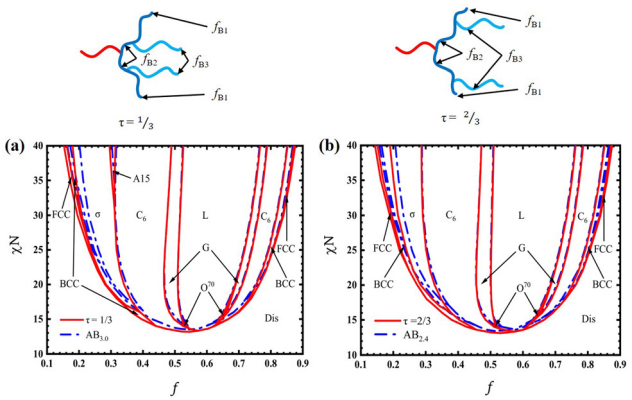

Fig. 4 Phase diagrams of: (a) the linear-hyperbranched copolymer with $f_{B3} = f_B/4$ for τ = 1/3 (red solid) and AB_4 copolymer with n_{equ} = 3.0 (simply denoted as $AB_{3.0}$, blue dot-dashed lines); (b) the linear-hyperbranched copolymer with $f_{B3} = f_B/4$ for τ = 2/3 (red solid) and AB_4 copolymer with n_{equ} = 2.4 (denoted as $AB_{2.4}$, blue dot-dashed lines). The length percentages of the B-blocks of all considered samples are listed in Table 2.

interface to the central area of the B-domain. Obviously, as the B3-blocks move from the junction point toward the free ends of the B1-blocks, the extension distance of the B-blocks increases, lowering the tendency of the B-blocks to locate outside the curvature. In other words, the effect of spontaneous curvature bending toward the A-domain is reduced with increasing τ, lowering the asymmetry of the phase diagram. In order to quantify the change in the asymmetry of the phase diagram with τ, we attempt to estimate the equivalent number of arms (n_{equ}[51]) by comparing the phase boundaries of the linear-hyperbranched copolymer with those of AB_n of unequal B arms. As the linear-hyperbranched architecture changes from AB_4 to AB_2 as τ increases from 0 to 1, its n_{equ} should accordingly decrease from 4 to 2. Therefore, we choose n = 4 and consider four arms containing two equal long arms with a segment number of $f_{B_l}N$ and two equal short arms with a segment number of $f_{B_s}N$. By tuning the relative lengths of the long and short arms of AB_4, we can get any value of $n_{equ} = n/iĐ$, where $iĐ = 2(k^2 + 1)/(k + 1)^2$ is the intramolecular polydispersity index[51] of the four arms of AB_4 with $k = f_{B_l}/f_{B_s}$. By minimizing the difference of the phase boundaries between the linear-hyperbranched copolymer with a given τ and AB_4 of unequal arms with respect to n_{equ} (or iĐ), we can obtain the value of n_{equ} quantifying the asymmetry of the linear-hyperbranched copolymer.

When minimizing the difference of the phase boundaries in the phase diagrams with respect to f and χN between the linear-hyperbranched copolymer and the AB_4 copolymer of unequal B arms with tunable n_{equ} or iĐ, we find it difficult to make all the boundaries between them perfectly consistent. The main reason is that the asymmetric architecture affects the deflection of different phase boundaries in different degrees. Accordingly, we estimate n_{equ} by mainly minimizing the sphere/cylinder, cylinder/gyroid and gyroid/lamella boundaries between the two copolymers in the region where A-blocks are located inside the curvature of the A/B interface, but not considering the sphere/disorder boundary. Fig. 4 presents the comparison of the phase diagrams between the linear-hyperbranched copolymer and the AB_4 copolymer of unequal B arms with optimized n_{equ} for τ = 1/3 and τ = 2/3. For τ = 1/3, the optimal n_{equ} is estimated around 3.0. In Fig. 4(a), the left C_6/G and G/L phase boundaries of the linear-hyperbranched copolymer with τ = 1/3 are nearly overlapped with those of AB_4 with n_{equ} = 3.0, and the σ/A15, σ/C_6 and A15/C_6 phase boundaries are also in good agreement with those of the latter. In contrast, the BCC/σ, BCC/FCC and FCC/disorder boundaries between the two copolymers are noticeably different. Another factor that should not be ignored is the difference in the equivalent segregation strength[89] between the copolymers, which has a considerable influence on the order–disorder (ODT) transition boundaries.[44,48] Nevertheless, the overall agreement of the phase boundaries between the two copolymers is acceptable. Therefore, it is a feasible approach to quantify the asymmetry of the phase diagram of the complex linear-hyperbranched copolymer using the equivalent number of arms defined by AB_n of unequal B arms.

In Table 1, we estimate the values of n_{equ} for $f_{B3} = f_B/4$ with τ = 0.1, 0.2, …, 0.9. Fig. 5(a) suggests that n_{equ} decreases nonlinearly as τ increases from 0 to 1. Since many phase boundaries need to be determined using SCFT for the estimation of each n_{equ}, the calculation is rather costly. To obtain the continuous value of n_{equ}, it would be useful to find an expression for n_{equ} as a function of τ. According to the changing trend, we choose the following concise equation to calculate n_{equ} of linear-hyperbranched copolymers,

$$n_{equ} = n_{min} + \Delta n \times (1 - \tau)^{\alpha}, \quad (10)$$

where $\Delta n = n_{max} - n_{min}$ and $\tau = f_{B2}/(f_{B2} + f_{B1})$. The copolymers with $n_{equ} = n_{max} = 4$ and $n_{min} = 2$ correspond to two limiting cases, τ = 0 and τ = 1, respectively. α is a constant that quantifies the nonlinear relationship between n_{equ} and τ. By fitting the data points in Fig. 5(a) using the expression, we got $\alpha \approx 1.6$. As τ decreases from 1 to 0, the increasing of n_{equ} along the fitting curve with α = 1.6 shown by the red solid lines in Fig. 5(a) is accelerating, causing the value of n_{equ} on the curve to be

Table 1 List of estimated n_{equ} and calculated n_{equ} for linear-hyperbranched copolymers with different τ

$f_{B3} = f_B/4$		
τ	Estimated n_{equ}	n_{equ} with $\alpha = 1.6$
0.1	3.63	3.69
0.2	3.32	3.40
0.3	3.06	3.13
0.4	2.84	2.88
0.5	2.65	2.66
0.6	2.50	2.46
0.7	2.36	2.29
0.8	2.24	2.15
0.9	2.13	2.05
$f_{B3} = f_B/6$		
τ	Estimated n_{equ}	n_{equ} with $\alpha = 1.6$
0.1	3.35	3.35
0.2	3.10	3.12
0.3	2.87	2.90
0.4	2.67	2.71
0.5	2.50	2.53
0.6	2.36	2.37
0.7	2.25	2.23
0.8	2.16	2.12
0.9	2.10	2.04

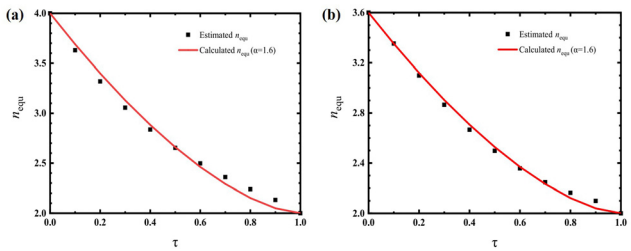

Fig. 5 Comparison of estimated n_{equ} by matching the phase boundaries (filled squares) and calculated n_{equ} using the expression of eqn (10) for linear-hyperbranched copolymers with different τ, $\alpha = 1.6$ (red solid) for: (a) $f_{B3} = f_B/4$; (b) $f_{B3} = f_B/6$.

smaller than the data points for $\tau \gtrsim 0.5$, then becomes larger than the data points for $\tau \lesssim 0.5$. Overall, the fitting curve with $\alpha = 1.6$ is in good agreement with those data points.

Similarly, we estimate the values of n_{equ} by the matching approach for $f_{B3} = f_B/6$ listed in Table 1. Using the expression in eqn (10) to fit these data points, we also obtain $\alpha \approx 1.6$. The fitting curve and the data points plotted in Fig. 5(b) show good agreement. These results demonstrate that n_{equ} of the linear-hyperbranched copolymer with varying architectures can be roughly estimated using the expression of eqn (10). Note that the linear-hyperbranched copolymer with $f_{B3} = f_B/6$ and $\tau = 0.5$ becomes the three-generation linear-dendrimer architecture (*i.e.* $g = 3$) with equal B-blocks and its asymmetric effect on the spontaneous curvature can be roughly quantified by the $n_{equ} \approx 2.5$ intermediate between those of AB_2 and AB_3 copolymers.

To understand how the asymmetric effect of the linear-dendrimer copolymer on the spontaneous curvature or the

Table 2 List of f_{B_i}/f_B for the considered linear-hyperbranched copolymers or AB_n

Copolymer	f_{B1}/f_B (%)	f_{B2}/f_B (%)	f_{B3}/f_B (%)	f_{B4}/f_B (%)
$\tau = 1/3$	16.7	8.3	25	—
$\tau = 2/3$	8.3	16.7	25	—
$AB_{2.4}$	4.6	4.6	45.4	45.4
$AB_{3.0}$	10.6	10.6	39.4	39.4
$AB_{3.2}$	12.5	12.5	37.5	37.5
$AB_{3.3}$	13.5	13.5	36.5	36.5
$AB_{3.8}$	19.2	19.2	30.8	30.8
$AB_{3.9}$	21.0	21.0	29.0	29.0

phase boundaries changes with increasing g, we directly estimate n_{equ} using the matching approach for $g = 4$ and $g = 5$, respectively. In Fig. 6(a), we calculated the sphere/cylinder/gyroid/lamella boundaries of AB_4 with unequal arms in the range of $25 \leq \chi N \leq 40$ as well as those of the linear-dendrimer copolymer with $g = 4$. For AB_4, we consider two samples with $n_{equ} = 3.20$ and $n_{equ} = 3.30$. The comparison of the phase boundaries suggests that the phase boundaries of AB_4 with $n_{equ} = 3.20$ are in good agreement with those of the linear-dendrimer copolymer with $g = 4$, and are noticeably better than those of AB_4 with $n_{equ} = 3.30$. Accordingly, we quantify the asymmetric effect of the linear-dendrimer copolymer with $g = 4$ to be $n_{equ} \approx 3.20$. Similarly, we estimate $n_{equ} \approx 3.80$ for the linear-dendrimer copolymer with $g = 5$.

In Fig. 7(a), we plot the estimated n_{equ} of the different linear-dendrimer copolymers with respect to g. When $g = 2$ increases to $g = 3$, the B-blocks at the outermost generation increase from 2 to 4, only raising $n = 2$ to $n_{equ} \approx 2.5$. In other words, the asymmetric effect of the linear-dendrimer copolymer with $g = 3$ is lower than that of AB_3 with equal arms. When $g = 3$ changes to $g = 4$, eight B-blocks are added at the outmost generation, while $n_{equ} \approx 2.5$ increases to $n_{equ} \approx 3.2$. These results demonstrate that the addition of these B-blocks at the outer generation has less effect on the asymmetry. For the AB_n copolymer, the packing of B-blocks nearby the A/B interface is very crowded, so it forces the interface to bend toward the A-block. The curved interface generates more space for the multiple B-blocks, thus reducing their stretching degree. In contrast, as the generation of the linear-dendrimer copolymer increases, B-blocks are added to the outermost generation while keeping

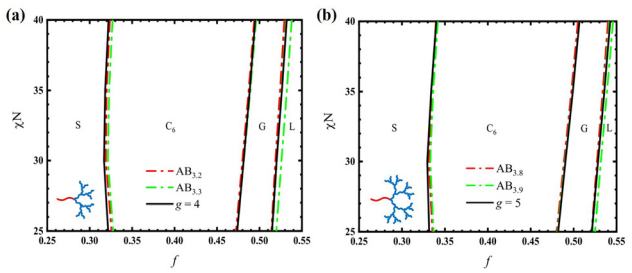

Fig. 6 Partial phase boundaries of: (a) $AB_{3.2}$ (red dot-dashed lines), $AB_{3.3}$ (green dot-dashed lines), and the linear-dendrimer copolymer with $g = 4$ (solid lines); (b) $AB_{3.8}$ (red dot-dashed lines), $AB_{3.9}$ (green dot-dashed lines), and the linear-dendrimer copolymer with $g = 5$ (solid lines). The length percentages of the B-blocks for all considered AB_n are listed in Table 2.

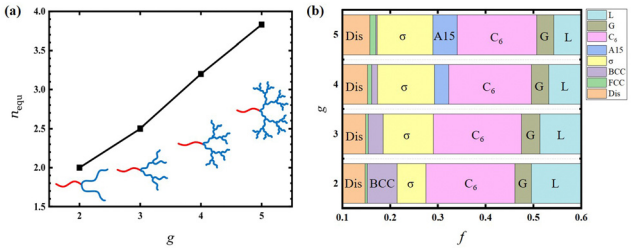

Fig. 7 (a) Variation of estimated n_{equ} for different linear-dendrimer copolymers with g = 2, 3, 4 and 5; (b) comparison of the disorder/FCC/BCC/Frank–Kasper/C_6/G/L phase boundaries of these different linear-dendrimer copolymers at χN = 40.

the B-blocks directly joined with the single A-block unchanged. In particular, as these B-blocks move away from the A/B junction or the A/B curved interface, they can access expanding space and thus they have less effect on the curvature. Even for g = 5 with sixteen B-blocks at the outermost generation, its asymmetric effect on the phase diagram is still lower than that of AB_4 with equal arms because of $n_{equ} \approx 3.8$.

Previous works[42,44,47,48,51] have shown that the architectural asymmetry of the block copolymer is commonly encoded into its phase diagram, leading to an expansion of the spherical phase region on one side and a compression on the opposite side. In the widened spherical region, complex Frank–Kasper phases tend to appear. Our previous work[51] on asymmetric AB_n copolymers with unequal B-arms demonstrated that the emergence of Frank–Kasper phases could be quantitatively indicated by the value of n_{equ}. Specifically, the Frank–Kasper σ-phase appears when $n_{equ} \gtrsim 1.5$, while the another Frank–Kasper A15-phase starts to emerge for $n_{equ} \gtrsim 2.5$. To further confirm that such conclusions also hold for the linear-dendrimer copolymers, we calculated the disorder/FCC/BCC/Frank–Kasper/C_6/G/L phase boundaries for the linear-dendrimer copolymers with g = 2, 3, 4, and 5 at χN = 40, as shown in Fig. 7(b). In the phase sequence of g = 3, there is a wide region of σ-phase but no A15 phase region due to $n_{equ} \approx 2.5$. For g = 4 with $n_{equ} \approx 3.2 > 2.5$, there exists a considerable region of A15-phase.

4 Conclusion

In summary, we have investigated the self-assembly behaviors of linear-hyperbranched copolymers using self-consistent field theory (SCFT). Firstly, we view the three-generation linear-hyperbranched copolymers as the derivatives of AB_n with equal or unequal B-arms. Different linear-hyperbranched copolymers are generated by moving two B-blocks along the arms of AB_2, and their equivalent arm numbers n_{equ} are estimated by comparing their phase boundaries with those of AB_n copolymers with unequal B-arms. The result of $2 \leq n_{equ} \leq 4$ suggests that their asymmetric effect on the spontaneous curvature or the deflection of phase boundaries, which is intermediate between those of AB_2 and AB_4 copolymers, is dependent on the tethering distance from the A/B junction point.

Then we turn to study the asymmetric effect of the linear-dendrimer copolymers composed of linear A-block as the first generation and equal B-block on the outer $g-1$ generations. Note that the linear-dendrimer copolymer with g = 2 is AB_2. For g = 3, 4 and 5, the equivalent arm numbers are estimated as $n_{equ} \approx 2.5$, 3.2 and 3.8, respectively. The changing tendency of n_{equ} with g indicates that the addition of B-blocks at the outer generation has less effect on the spontaneous curvature because they are further from the A/B junction. The asymmetric effect of the linear-dendrimer copolymer quantified by the value of n_{equ} is confirmed by the changing trend of these spherical phase regions. Specifically, the phase sequence of g = 3 contains Frank–Kasper σ-phase but no A15-phase because $n_{equ} \approx 2.5$ is close to the critical value of n_{equ} for the emergence of A15. Since n_{equ} increases to about 3.2 for g = 4, a noticeable region of A15 appears in the phase sequence. Our work provides a comprehensive understanding of the asymmetric effect on the phase boundaries for linear-hyperbranched copolymers.

Data availability

Isosurface plots and the corresponding parameters of the candidate ordered phases considered in the current study are available in the ESI.†

Conflicts of interest

There are no conflicts to declare.

Acknowledgements

This work was supported by the National Natural Science Foundation of China (Grant No. 22333002, 21925301, 22203018, 22163006).

References

1 F. S. Bates, M. A. Hillmyer, T. P. Lodge, C. M. Bates, K. T. Delaney and G. H. Fredrickson, *Science*, 2012, **336**, 434–440.
2 F. S. Bates and G. H. Fredrickson, *Phys. Today*, 1999, **52**, 32–38.
3 M. W. Matsen and F. S. Bates, *Macromolecules*, 1996, **29**, 1091–1098.
4 M. W. Matsen and F. S. Bates, *Macromolecules*, 1996, **29**, 7641–7644.
5 H. Y. Hsueh, C. T. Yao and R. M. Ho, *Chem. Soc. Rev.*, 2015, **44**, 1974–2018.
6 M. Stefik, S. Guldin, S. Vignolini, U. Wiesner and U. Steiner, *Chem. Soc. Rev.*, 2015, **44**, 5076–5091.
7 M. Radjabian and V. Abetz, *Prog. Polym. Sci.*, 2020, **102**, 101219.
8 Z. W. Xu, Q. S. Dong and W. H. Li, *Macromolecules*, 2024, **57**, 1869–1884.
9 F. Drolet and G. H. Fredrickson, *Phys. Rev. Lett.*, 1999, **83**, 4317–4320.
10 T. S. Bailey, C. M. Hardy, T. H. Epps and F. S. Bates, *Macromolecules*, 2002, **35**, 7007–7017.

11 H. L. Deng, Y. C. Qiang, T. T. Zhang, W. H. Li and T. Yang, *Nanoscale*, 2016, **8**, 15961–15969.
12 T. H. Epps, E. W. Cochran, T. S. Bailey, R. S. Waletzko, C. M. Hardy and F. S. Bates, *Macromolecules*, 2004, **37**, 8325–8341.
13 C. A. Tyler and D. C. Morse, *Phys. Rev. Lett.*, 2005, **94**, 208302.
14 Z. W. Xu, Q. S. Dong, L. S. Zhang and W. H. Li, *Nanoscale*, 2022, **14**, 15275–15280.
15 C. H. Huang, Y. Y. Zhu and X. K. Man, *Phys. Rep.*, 2021, **932**, 1–36.
16 M. Müller, *Prog. Polym. Sci.*, 2020, **101**, 101198.
17 E. Vargo, L. Ma, H. Li, Q. T. Zhang, J. Kwon, K. M. Evans, X. C. Tang, V. L. Tovmasyan, J. Jan, A. C. Arias, H. Destaillats, I. Kuzmenko, J. Ilavsky, W. R. Chen, W. Heller, R. O. Ritchie, Y. Liu and T. Xu, *Nature*, 2023, **623**, 724–731.
18 T. Y. Tang, H. L. Wang, C. T. Yao, K. C. Yang, R. M. Ho and D. H. Tsai, *Nanoscale*, 2018, **10**, 7352–7356.
19 Y. W. Harn, S. Liang, S. L. Liu, Y. Yan, Z. W. Wang, J. Jiang, J. W. Zhang, Q. Li, Y. J. He, Z. L. Li, L. Zhu, H. P. Cheng and Z. Q. Lin, *Proc. Natl. Acad. Sci. U. S. A.*, 2021, **118**, 1–11.
20 B. Wang, C. Wang, X. W. Yu, Y. Cao, L. F. Gao, C. P. Wu, Y. F. Yao, Z. Q. Lin and Z. G. Zou, *Nat. Synth.*, 2022, **1**, 138–146.
21 H. Hasegawa, H. Tanaka, K. Yamasaki and T. Hashimoto, *Macromolecules*, 1987, **20**, 1651–1662.
22 S. Foerster, A. K. Khandpur, J. Zhao, F. S. Bates, I. W. Hamley, A. J. Ryan and W. Bras, *Macromolecules*, 1994, **27**, 6922–6935.
23 D. A. Hajduk, P. E. Harper, S. M. Gruner, C. C. Honeker, G. Kim, E. L. Thomas and L. J. Fetters, *Macromolecules*, 1994, **27**, 4063–4075.
24 M. W. Matsen and M. Schick, *Phys. Rev. Lett.*, 1994, **72**, 2660–2663.
25 A. K. Khandpur, S. Foerster, F. S. Bates, I. W. Hamley, A. J. Ryan, W. Bras, K. Almdal and K. Mortensen, *Macromolecules*, 1995, **28**, 8796–8806.
26 D. Yamaguchi, T. Hashimoto, N. Y. Vaidya and C. D. Han, *Macromolecules*, 1999, **32**, 7696–7699.
27 E. W. Cochran, C. J. Garcia-Cervera and G. H. Fredrickson, *Macromolecules*, 2006, **39**, 4264.
28 Y. Y. Huang, J. Y. Hsu, H. L. Chen and T. Hashimoto, *Macromolecules*, 2007, **40**, 406–409.
29 K. Kimishima, K. Saijo, T. Koga and T. Hashimoto, *Macromolecules*, 2013, **46**, 9032–9044.
30 C. H. Lin, T. Higuchi, H. L. Chen, J. C. Tsai, H. Jinnai and T. Hashimoto, *Macromolecules*, 2018, **51**, 4049–4058.
31 M. W. Matsen, *Macromolecules*, 2012, **45**, 2161–2165.
32 K. Almdal, K. A. Koppi, F. S. Bates and K. Mortensen, *Macromolecules*, 1992, **25**, 1743–1751.
33 J. D. Vavasour and M. D. Whitmore, *Macromolecules*, 1993, **26**, 7070–7075.
34 F. S. Bates, M. F. Schulz, A. K. Khandpur, S. Foerster, J. H. Rosedale, K. Almdal and K. Mortensen, *Faraday Discuss.*, 1994, **98**, 7–18.
35 M. W. Matsen and M. Schick, *Macromolecules*, 1994, **27**, 4014–4015.
36 M. W. Matsen and F. S. Bates, *J. Polym. Sci., Part B:Polym. Phys.*, 1997, **35**, 945–952.
37 M. W. Bates, J. Lequieu, S. M. Barbon, R. M. Lewis, K. T. Delaney, A. Anastasaki, C. J. Hawker, G. H. Fredrickson and C. M. Bates, *Proc. Natl. Acad. Sci. U. S. A.*, 2019, **116**, 13194–13199.
38 K. D. Dorfman, *Macromolecules*, 2021, **54**, 10251–10270.
39 Y. C. Xu, W. H. Li, F. Qiu and Z. Q. Lin, *Nanoscale*, 2014, **6**, 6844–6852.
40 J. Park, S. Jang and J. K. Kim, *J. Polym. Sci., Part B:Polym. Phys.*, 2015, **53**, 1–21.
41 Y. C. Qiang, W. H. Li and A. C. Shi, *ACS Macro Lett.*, 2020, **9**, 668–673.
42 G. M. Grason and R. D. Kamien, *Phys. Rev. E:Stat., Nonlinear, Soft Matter Phys.*, 2005, **71**, 051801.
43 W. Li and Y. X. Liu, *J. Chem. Phys.*, 2021, **154**, 014903.
44 D. L. Vigil, T. Quah, D. Sun, K. T. Delaney and G. H. Fredrickson, *Macromolecules*, 2022, **55**, 4237–4244.
45 J. Lequieu, T. Koeper, K. T. Delaney and G. H. Fredrickson, *Macromolecules*, 2020, **53**, 513–552.
46 G. M. Grason, B. A. DiDonna and R. D. Kamien, *Phys. Rev. Lett.*, 2003, **91**, 058304.
47 G. M. Grason and R. D. Kamien, *Macromolecules*, 2004, **37**, 7371–7380.
48 N. Xie, W. H. Li, F. Qiu and A. C. Shi, *ACS Macro Lett.*, 2014, **3**, 906–910.
49 Z. H. Gan, D. D. Zhou, Z. Ma, M. Xu, Z. Q. Xu, J. W. He, J. J. Zhou and X. H. Dong, *J. Am. Chem. Soc.*, 2022, **145**, 487–497.
50 S. T. Milner, *Macromolecules*, 1994, **27**, 2333–2335.
51 J. H. Shi, X. B. Huang and W. H. Li, *Phys. Chem. Chem. Phys.*, 2023, **25**, 20032–20041.
52 X. Y. Feng, G. X. Liu, D. Guo, K. N. Lang, R. M. Zhang, J. H. Huang, Z. B. Su, Y. W. Li, M. J. Huang, T. Li and S. Z. D. Cheng, *ACS Macro Lett.*, 2019, **8**, 875–881.
53 S. Lee, M. J. Bluemle and F. S. Bates, *Science*, 2010, **330**, 349–353.
54 Y. C. Liu, H. Y. Lei, Q. Y. Guo, X. Y. Liu, X. H. Li, Y. A. Wu, W. Y. Li, W. Zhang, G. X. Liu, X. Y. Yan and S. Z. D. Cheng, *Chin. J. Polym. Sci.*, 2023, **41**, 607–620.
55 X. Y. Yan, Y. C. Liu, X. Y. Liu, H. Y. Lei, X. H. Li, Y. C. Wang, W. Y. Li, Q. Y. Guo, M. J. Huang and S. Z. D. Cheng, *Phys. Rev. Mater.*, 2023, **7**, 120302.
56 F. S. Bates and G. H. Fredrickson, *Macromolecules*, 1994, **27**, 1065–1067.
57 M. W. Schulze, R. M. Lewis, J. H. Lettow, R. J. Hickey, T. M. Gillard, M. A. Hillmyer and F. S. Bates, *Phys. Rev. Lett.*, 2017, **118**, 207801.
58 M. W. Bates, S. M. Barbon, A. E. Levi, R. M. Lewis, H. K. Beech, K. M. Vonk, C. Zhang, G. H. Fredrickson, C. J. Hawker and C. M. Bates, *ACS Macro Lett.*, 2020, **9**, 396–403.
59 S. M. Barbon, J. A. Song, D. Y. Chen, C. Zhang, J. Lequieu, K. T. Delaney, A. Anastasaki, M. Rolland, G. H. Fredrickson,

M. W. Bates, C. M. Hawker and C. J. Bates, *Macromolecules*, 2020, **9**, 1745–1752.
60 Z. Ma, R. Tan, Z. H. Gan, D. D. Zhou, Y. D. Yang, W. Zhang and X.-H. Dong, *Macromolecules*, 2022, **55**, 4331–4340.
61 E. B. Zhulina, S. S. Sheiko, A. V. Dobrynin and O. V. Borisov, *Macromolecules*, 2020, **53**, 2582–2593.
62 Z. Ma, D. D. Zhou, M. Xu, Z. H. Gan, T. Y. Zheng, S. Wang, R. Tan and X.-H. Dong, *Macromolecules*, 2023, **56**, 833–840.
63 R. J. Sánchez-Leija, J. A. Mysona, J. J. de Pablo and P. F. Nealey, *Macromolecules*, 2024, **57**, 2019–2029.
64 V. Percec, C. H. Ahn, G. Ungar, D. J. P. Yeardley, M. Moller and S. S. Sheiko, *Nature*, 1998, **391**, 161–164.
65 B. K. Cho, A. Jain, S. M. Gruner and U. Wiesner, *Science*, 2004, **305**, 1598–1601.
66 A. G. Marcos, T. M. Pusel, R. Thomann, T. Pakula, L. Okrasa, S. Geppert, W. Gronski and H. Frey, *Macromolecules*, 2006, **39**, 971–977.
67 Y. W. Chung, J. K. Lee, W. C. Zin and B. K. Cho, *J. Am. Chem. Soc.*, 2008, **130**, 7139–7147.
68 W. M. Wan and C. Y. Pan, *Macromolecules*, 2008, **41**, 5085–5088.
69 F. Wurm, H. Schüle and H. Frey, *Macromolecules*, 2008, **41**, 9602–9611.
70 F. Wurm, J. Klos, H. J. Räder and H. Frey, *J. Am. Chem. Soc.*, 2009, **131**, 7954–7955.
71 A. M. Hofmann, F. Wurm, E. Hühn, T. Nawroth, P. Langguth and H. Frey, *Biomacromolecules*, 2010, **11**, 568–574.
72 Y. Q. Xu, P. Xiang, Z. B. Ye and W. J. Wang, *Macromolecules*, 2010, **43**, 8026–8038.
73 X. J. Zhang, J. A. Cheng, Q. R. Wang, Z. L. Zhong and R. X. Zhuo, *Macromolecules*, 2010, **43**, 6671–6677.
74 C. Schüll, H. Rabbel, F. Schmid and H. Frey, *Macromolecules*, 2013, **46**, 5823–5830.
75 Y. Shi, X. S. Cao, S. J. Luo, X. F. Wang, R. W. Graff, D. Q. Hu, R. L. Guo and H. F. Gao, *Macromolecules*, 2016, **49**, 4416–4422.
76 F. Li, M. X. Cao, Y. J. Feng, R. Q. Liang, X. W. Fu and M. J. Zhong, *J. Am. Chem. Soc.*, 2019, **141**, 794–799.
77 T. Jun, H. Park, S. Jeon, H. Ahn, W. D. Jang, B. Lee and D. Y. Ryu, *Nanoscale*, 2022, **14**, 16936–16943.
78 T. Jun, H. Park, J. Kim, W. Lee, H. Ahn, W. D. Jang, B. Lee and D. Ryu, *Nanoscale*, 2023, **15**, 9069–9075.
79 M. W. Matsen, *J. Phys.: Condens. Matter*, 2002, **14**, R21–R47.
80 G. H. Fredrickson, *The Equilibrium Theory of Inhomogeneous Polymers*, Oxford University Press, 2006.
81 G. Tzeremes, K. O. Rasmussen, T. Lookman and A. Saxena, *Phys. Rev. E:Stat., Nonlinear, Soft Matter Phys.*, 2002, **65**, 041806.
82 K. O. Rasmussen and G. Kalosakas, *J. Polym. Sci., Part B:Polym. Phys.*, 2002, **40**, 1777–1783.
83 P. Stasiak and M. W. Matsen, *Eur. Phys. J. E:Soft Matter Biol. Phys.*, 2011, **34**, 110.
84 R. B. Thompson, K. O. Rasmussen and T. Lookman, *J. Chem. Phys.*, 2004, **120**, 31–34.
85 C. A. Tyler and D. C. Morse, *Macromolecules*, 2003, **36**, 8184–8188.
86 A. Arora, D. C. Morse, F. S. Bates and K. D. Dorfman, *J. Chem. Phys.*, 2017, **146**, 244902.
87 J. Qin, *PhD thesis*, The University of Minnesota, Minneapolis, USA, 2009.
88 Y. C. Qiang and W. H. Li, *Macromolecules*, 2020, **53**, 9943–9952.
89 X. W. Ji and W. H. Li, *Phys. Chem. Chem. Phys.*, 2020, **22**, 17824–17832.

